Photophysical properties of tetraphenylporphyrin-subphthalocyanine conjugates

Muthumuni Managa,[a] John Mack,[a,*] Daniel Gonzalez-Lucas,[b] Sonia Remiro-Buenamañana,[b] Charmaine Tshangana,[a] Andrew N. Cammidge[b,*] and Tebello Nyokong[a,*]

[a] *Department of Chemistry, Rhodes University, Grahamstown 6140, South Africa*

[b] *School of Chemistry, University of East Anglia, Norwich NR4 7TJ, UK*

This paper is dedicated to Professor Kevin Smith on the occasion of his 70th birthday.

Received date (to be automatically inserted after your manuscript is submitted)

Accepted date (to be automatically inserted after your manuscript is accepted)

ABSTRACT: Novel tetraphenylporphyrin-subphthalocyanine conjugates have been prepared and characterized. An analysis of their optical spectroscopy and electronic structures using fluorescence emission and MCD spectroscopy and TD-DFT calculations, demonstrates that the two chromophores do not interact to any significant extent.

KEYWORDS: porphyrins, subphthalocyanines, MCD spectroscopy, TD-DFT calculations, singlet oxygen

*Correspondence to: John Mack, email: j.mack@ru.ac.za, Tel: +27 46-603-7234; Andrew Cammidge, email: a.cammidge@uea.ac.uk, Tel: +44 1603 592011; Tebello Nyokong, email: t.nyokong@ru.ac.za, Tel: +27 46-603-8801.

INTRODUCTION

Porphyrins are an important class of dyes and can be of natural or synthetic origin. Those that are naturally occurring are important in biological systems and play a central role in photosynthesis, biological oxidation and reductions and transport of oxygen by haemoglobin [1, 2]. There has been a strong research focus on synthetic porphyrins for many decades due to a wide range of possible applications, such as photodynamic antimicrobial chemotherapy (PACT) [3], optoelectronics, sensors [4] and photodynamic therapy (PDT) [2]. Many of these possible applications depend on the optical properties of the porphyrin π-system and the absorption of photons in the visible region. A key drawback of porphyrins in this regard is that the Q bands, which lie at the red end of the visible region tend be relatively weak, while the more intense B (or Soret) band lies in the 400–450 nm region [5]. The introduction of a second antenna chromophore with complementary absorbing features could address this issue and ideally would result in the formation of a "black chromophore" [6] that absorbs across the entire

visible region. The para-substituents at the *meso*-carbons of tetraphenylporphyrin (TPP) are an obvious point of attachment for such a chromophore. 5-(4-Hydroxyphenyl)-10,15,20-triphenylporphyrin **(H_2TPP-OH)** and its Zn(II) complex (**ZnTPP-OH**) were selected for study in this regard [7-9] with subphthalocyanine (subPc) as the antenna chromophore. SubPcs exhibit intense absorption and emission bands in the visible region [8, 9] and have similar potential applications to TPPs [7, 10]. In this study, the photophysical properties of oxygen-bridged porphyrin-subphthalocyanine (TPP-O-subPc) conjugates (Scheme 1) are studied in detail.

EXPERIMENTAL

Reagents

Tetraphenyl porphyrin (TPP) was purchased from Sigma. Propionic acid and methanol (MeOH) were purchased from Merck. Chloroform, dimethyl formamide (DMF) toluene and ethyl acetate were purchased from Minema chemicals. Petroleum ether (PET) was purchased from Saarchem and dichloromethane (DCM) was purchased from B&M Scientific. With the exception of pyrrole, which was distilled prior to use, all reagents were used as supplied.

Synthesis

Boron subphthalocyanine chloride (subPc) [11, 12], **H_2TPP-OH** [13] and **ZnTPP-OH** [14] were synthesized according to literature procedures.

Synthesis of the H_2TPP-O-subPc conjugate: H_2TPP-OH (7.8 mg, 10 μmol) and **subPc** (16 mg, 30 μmol) were dissolved in toluene (4 ml) and then introduced in to a sealable tube that was flushed with nitrogen prior to the reaction. The tube was sealed and the reaction mixture was stirred and heated on an oil bath at 140°C for 24 h. The product was purified by silica gel column chromatography using petroleum ether/ethyl acetate (4:1) as eluent. Yield: (60%). ^{1}H NMR (500 MHz, $CDCl_3$) δ (ppm) 9.00 – 8.93 (m, 6H), 8.85 – 8.80 (m, 4H), 8.75 (d, *J* = 4.7 Hz, 2H), 8.61 (d, *J* = 4.7 Hz, 2H), 8.24 – 8.16 (m, 6H), 8.00 – 7.90 (m, 6H), 7.80 – 7.70 (m, 9H), 7.59 (d, *J* = 8.2 Hz, 2H), 5.76 (d, *J* = 8.2 Hz, 2H) –2.51 (s, 2H). MALDI-TOF-MS m/z calc: 1024.93; Found: 1025.51.

Synthesis of the **ZnTPP-O-subPc** conjugate: Prepared as above using **ZnTPP-OH**. Yield: (69%). ^{1}H NMR (500 MHz, $CDCl_3$) δ (ppm) 9.00 – 8.90 (m, 10H), 8.86 (d, *J* = 4.7 Hz, 2H), 8.70 (d, *J* = 4.7 Hz, 2H), 8.25 – 8.17 (m, 6H), 7.97 – 7.95 (m, 6H), 7.80 – 7.71 (m, 9H), 7.59 (d, *J* = 8.3 Hz, 2H), 5.76 (d, *J* = 8.3 Hz, 2H). MALDI-TOF-MS m/z calc: 1086.32; Found: 1086.27.

Instrumentation

UV-visible absorption spectra were recorded at room temperature with a 1 cm pathlength cuvette on a Shimadzu UV-2550 spectrophotometer. Magnetic circular dichroism (MCD) spectra were measured with a Chirascan plus spectrodichrometer equipped with a 1 T (tesla) permanent magnet by using both the parallel and antiparallel fields. The conventions of Piepho and Schatz are used to describe the sign of the MCD signal and the Faraday terms [15]. Fluorescence emission and excitation spectra were collected on a Varian Eclipse spectrofluorimeter. The absorbance ranged between 0.04 and 0.05 at the excitation wavelength for all samples.

The singlet oxygen generation was directly quantified in DMF, in the absence and presence of sodium azide, a physical quencher for $^1O_2$, using an ultrasensitive germanium detector (Edinburgh Instruments, EI-P) combined with a 1000 nm long pass filter (Omega, 3RD 1000 CP) and a 1270 nm band pass filter (Omega, C1275, BP50) to detect the intensity of the phosphorescence band at 1270 nm. The detection direction is perpendicular to that of a 422 nm excitation beam from the optical parametric oscillator (OPO) unit of an Ekspla NT 342B-20-AW laser (2.0 mJ/5 ns, 20 Hz), which ran through a 1 cm quartz fluorescence cell holding the sample solution. The signal was averaged over 128 measurement pulses with a digital oscilloscope (Tektronix TDS 3032C) to obtain the dynamic decay curve for $^1O_2$ formation. Mass spectral data were collected with a Bruker AutoFLEX III Smartbeam TOF/TOF Mass spectrometer. ^1H and ^{13}C-NMR spectra were recorded at 500.1 and 125.7 MHz, respectively, using a Bruker AscendTM 500. The residual solvent peaks were used as references.

Theoretical Calculations

The density functional theory (DFT) method was used to carry out geometry optimizations for **subPc**, **H_2TPP-OH**, **ZnTPP-OH**, **H_2TPP-O-subPc** and **ZnTPP-O-subPc** by using the B3LYP functional of the Gaussian09 program package [16] with 6-31G(d) basis sets. The B3LYP functional was used with 6-31G(d) basis sets for the geometry optimizations. The same approach was used to calculate the electronic absorption properties based on the TD-DFT method. The CAM-B3LYP functional includes a long-range correction of the exchange potential, which incorporates an increasing fraction of Hartree–Fock (HF) exchange as the interelectronic separation increases

ELECTRONIC STRUCTURES OF PORPHYRINOIDS

Electronic absorption spectroscopy is one of the most useful methods for characterizing porphyrins and phthalocyanines and their analogues, due to the presence in each case of the intense Q and B bands of Gouterman's 4-orbital model [5] at the red and blue ends of the visible regions, respectively. A $C_{16}H_{16}^{2-}$ cyclic polyene corresponding to the inner ligand perimeter can be regarded as being the parent perimeter for describing and rationalizing the optical properties. In the context of tetrapyrrolic compounds the π-system contains a series of MOs arranged in ascending energy with M_L = 0, ±1, ±2, ±3, ±4, ±5, ±6, ±7 and 8 nodal properties based on the magnetic quantum number for the cyclic perimeter, M_L. The frontier π-MOs have M_L = ±4 and ±5 nodal properties, respectively. The four spin-allowed M_L = ±4 → ±5 excitations give rise to two orbitally degenerate ^1E_u excited states, on the basis of the ΔM_L = ±9, and ΔM_L = ±1 transitions. This results in the forbidden and allowed Q and B bands of Gouterman's 4-orbital model for porphyrins [5], since an incident photon can provide only one quantum of orbital angular momentum. Michl [17] introduced an **a**, **s**, **-a** and **-s** terminology (Fig. 1) for the four MOs derived from the HOMO and LUMO of the parent perimeter so that π-systems of porphyrinoids with differing molecular symmetries can be readily compared. One MO derived from the HOMO of a $C_{16}H_{16}^{2-}$ parent hydrocarbon perimeter and another derived from the LUMO have nodal planes which coincide with the *yz*-plane and are referred to, respectively, as the **a** and **-a** MOs, while the corresponding MOs with antinodes on the *yz*-plane are referred to as the **s** and **-s** MOs (Fig. 1). In a similar manner the frontier π-MOs of subPcs can be described as being derived from a $C_{12}H_{12}^{2-}$ parent perimeter with a M_L = 0, ±1, ±2, ±3, ±4, ±5, 6, and frontier π-MOs that have M_L = ±3 and ±4 nodal properties.

RESULTS AND DISCUSSION

Synthesis and Characterization

The synthesis of **H_2TPP-OH** and **ZnTPP-OH** enables the formation of TPP-O-subPc conjugates containing a single subPc antenna complex in the manner described recently by Berlin and coworkers [18] after the synthesis work in this study had been completed, through an exchange reaction of the hydroxyl para-substituent of one of the *meso*-phenyl rings with the chloride axial ligand. In contrast with the study of Berlin and coworkers [18], the parent boron subphthalocyanine chlorine complex was used rather than its perfluorinated analogues (Scheme 1). DFT geometry optimizations were carried out so that the conformation of the conjugate can be assessed. The TPP and subPc moieties are predicted to lie in an orthogonal arrangement, but there is scope for flexibility around the linking *meso*-phenyl ring (Fig. 2). Although the bridging oxygen atom is sp^3 hybridized there appeared to be scope for an interaction between the ring moieties, since the lone pairs can interact significantly with the π-system of the phenyl ring. For example, the recent spectroscopic characterization and theoretical analysis of a novel nickel 10-oxacorrole complex by Kobayashi and co-workers demonstrated that an sp^3 hybridized oxygen atom can form part of a cyclic π-system with properties very similar to those of a conventional 18-π-electron heteroaromatic π-system of a porphyrinoid ligand [19].

Optical spectroscopy and TD-DFT calculations

The electronic absorption spectra of the conjugates are dominated by the Q and B bands of the TPP and subPc chromophores (Fig. 3 and Table 1). The intense B band of the TPP chromophore in the 410-430 nm and the weaker lowest energy Q bands of **ZnTPP-OH** and **H_2TPP-OH** at ca. 600 and 650 nm, respectively, can be readily assigned in the spectra of the conjugates. The Q band of the subPc chromophore is slightly blue shifted to 562 nm on coordination to both porphyrins. Magnetic circular dichroism (MCD) spectroscopy can be used to identify the main electronic $Q_{(0,0)}$ and $B_{(0,0)}$ bands of porphyrinoids, due to the presence of intense Faraday $\mathcal{A}_1$ terms or coupled pairs of oppositely-signed Faraday $\mathcal{B}_0$ terms [20, 21]. In the context of the TPP-O-subPc conjugates, the two chromophores can be viewed as retaining their four-fold and three-fold axes of symmetry, since they are linked at the axial position of the boron atom of subPc and a *meso*-phenyl ring of TPP rather than being directly linked to the two core chromophores, so the spectra are dominated by pseudo-$\mathcal{A}_1$ terms.

DFT and TD-DFT were carried out to analyze trends in the electronic structures and optical spectra. The trends in the calculated spectra are fully consistent with the experimental data (Fig. 3 and Table 2). A comparison with the trends predicted for **subPc**, **ZnTPP-OH** and **H_2TPP-OH**, demonstrates that the MO energies of the frontier π-MOs of the subPc and TPP chromophores are almost unchanged when the **H_2TPP-O-subPc** and **ZnTPP-O-subPc** conjugates are formed (Fig. 4) resulting in near identical HOMO–LUMO gaps and hence predicted Q and B band energies (Fig. 3 and Table 1). The only significant change is a slight destabilization of the **s** MOs, which have large MO coefficients on the *meso*-carbons of the TPP ring moieties of **H_2TPP-O-subPc** and **ZnTPP-O-subPc** (Fig. 1). Since the **a** and **s** MOs of **subPc** have angular nodal planes on alternating sets of atoms (Fig. 1), the incorporation of the aza-nitrogen atoms have a much larger stabilizing effect on the energy of the **s** MO resulting in a large separation of the **a** and **s** MOs (the ΔHOMO value in the context of Michl's perimeter model [17]) and $Q_{(0,0)}$ bands that are dominated by the **a** →

-a and **a** → **-s** one-electron transitions (Table 2) rather than having near equal contributions from the **s** → **-a** and **s** → **-s** one-electron transitions [5, 22]. This leads to a mixing of the allowed and forbidden properties of the Q and B bands resulting in the observed significant absorption intensity for the **subPc** Q band in the 550–600 nm region.

In order to assess whether the conjugates act as one molecule in electronic terms a series of fluorescence emission spectra were measured at different excitation wavelengths and a marked wavelength dependence was observed (Fig. 5). Porphyrins emission occurs with two peaks as shown in Fig. 5. Upon excitation at 418 nm where the TPP chromophore absorbs strongly and subPc absorbs weakly, only emission that is consistent with the presence of the TPP chromophore is observed at 610 and 656 nm (Fig. 5). In contrast, exciting at 548 nm, where the main peak for SubPc is located, resulted mainly in **SubPc** emission at 600 nm. Thus, the emission bands for both the subPc and TPP fluorophores are observed in the spectra measured for the conjugates, which demonstrates that the two macrocyclic rings act independently in electronic terms.

Singlet oxygen quantum yield studies

Time-resolved phosphorescence decay curves for singlet oxygen were used to determine singlet oxygen quantum yields for **H_2TPP-O-subPc** and **ZnTPP-O-subPc** in DMF using Eq. (1) [23]:

$$I(t) = B\frac{\tau_D}{\tau_T - \tau_D}[e^{-t/\tau_T} - e^{-t/\tau_D}] \quad (1)$$

where, $I_{(t)}$ is the phosphorescence intensity of $^1O_2$ at time t, τ_D is the lifetime of the $^1O_2$ phosphorescence decay, τ_T is the triplet state lifetime of the standard or sample and B is a coefficient associated with the sensitizer concentration and $^1O_2$ quantum yield. The singlet oxygen quantum yield, Φ_Δ of the complex was then determined in aqueous media, using Eq. (2):

$$\Phi_\Delta = \Phi_\Delta^{(Std)} . \frac{B.A^{(Std)}}{B^{(Std)}.A} \quad (2)$$

where $\Phi_\Delta^{(Std)}$ is the singlet oxygen quantum yield for the standard Rose Bengal (0.47 in DMF [24]), B and $B^{(Std)}$ refer to a coefficient related to the sensitizer concentration and the $^1O_2$ quantum yield for the sample and standard, respectively; while A and $A^{(Std)}$ refer to the absorbance values at the excitation wavelengths shown in Table 2. The Φ_Δ values for the conjugates are consistently lower than what is observed for the **subPc**, **H_2TPP-OH** and **ZnTPP-OH**. The Φ_Δ values in DMF for **subPc**, **H_2TPP-OH** and **ZnTPP-OH** are Φ_Δ = 0.76, 0.57 and 0.75, respectively, Table 1. The higher Φ_Δ value for **ZnTPP-OH** is due to the heavy atom effect. A marked wavelength dependence is observed in the Φ_Δ values for **H_2TPP-O-subPc** and **ZnTPP-O-subPc** as would be anticipated for two chromophores, which do not interact with each other (Table 1). When the conjugates are excited in the TPP B band (418 nm or 426 nm for **H_2TPP-O-subPc** and **ZnTPP-O-subPc**, respectively), there is no difference in the Φ_Δ values for **H_2TPP-OH** and **H_2TPP-O-subPc**, but there is a large decrease in Φ_Δ value of **ZnTPP-O-subPc** relative to that of **ZnTPP-OH**. When the conjugates are excited in the SubPc Q band (562 nm and 532 nm for **H_2TPP-O-subPc** and **ZnTPP-O-subPc**, respectively), the Φ_Δ values decrease to 0.69 and 0.72, for **H_2TPP-O-subPc** and **ZnTPP-O-subPc**, respectively, from 0.76 for **SubPc**, Table

1. The most likely explanation is that additional conformational flexibility results in enhanced non-radiative decay pathways.

Fluorescence quantum yield

Fluorescence quantum yields (Φ_F) were quantified using the comparative method and were be determined by comparison with a standard using Eq. 3 [25]:

$$\Phi_F = \Phi_{F_{(Std)}} \frac{F.A_{(Std)}n^2}{F_{(Std)}.A.n^2_{(Std)}} \quad (3)$$

where $\Phi_{F(std)}$ is the fluorescence quantum yield for the ZnTPP standard (0.11 in DMF [5, 26]), F and $F_{(Std)}$ are the areas under the fluorescence curves for the sample and standard, respectively, while A and $A_{(Std)}$ are the absorbance values of the sample and standard at the excitation wavelength respectively, and n and $n_{(Std)}$ are the refractive indices of solvents in which the sample and reference were dissolved. There is a general decrease in Φ_F values when exciting in the TPP B band and the subPc Q band (**H_2TPP-O-subPc** and **ZnTPP-O-subPc**) when the values are compared to those of **subPc**, **H_2TPP-OH** and **ZnTPP-OH**, since increased conformational flexibility can enhance the rate of nonradiative decay. In each case, a marked wavelength dependence is observed in the Φ_F values for the TPP-O-subPc conjugates as the excitation wavelength is varied (Table 1), which provides further evidence that two fluorophores act independently.

CONCLUSIONS

TPP-O-subPc conjugates linked by an sp^3-hybridized oxygen atom as the axial atom at the core boron atom of the subPc moieties have been successfully synthesized and characterized. The two ring systems are found to act independently during the photophysical measurements, which demonstrates that the subPc does not act as an antenna complex for the TPP ring. The high Φ_Δ values of both the TPP and subPc chromophores are retained, however, so there is still scope for utilizing a wider portion of the visible region for $^1O_2$ generation than is normally the case with a TPP complex, since the subPc Q band lies between the Q and B bands of the TPP chromophore.

Acknowledgements

This work was supported by the Department of Science and Technology (DST) Innovation and National Research Foundation (NRF), South Africa through DST/NRF South African Research Chairs Initiative (UID 62620), the Pearson Young Memorial Trust, and by the CSIR National Laser Centre, Rental Pool Programme. The theoretical calculations were carried out at the Centre for High Performance Computing in Cape Town, South Africa.

References

[1] Ryskova L, Buchta V and Slezak R. *Cent. Eur. J. Biol.* 2010; **5**: 400-406.

[2] Maisch T. *Laser Med. Sci.* 2007; **22**: 83-91.

[3] Malik Z, Hanania J and Nitzan Y. *J. Photochem Photobiol. B.* 1990; **5**: 281-293.

[4] Kadish KM, Smith KM and Guilard R. *Handbook of Porphyrin Science*, World Scientific, Singapore, 2010.

[5] Gouterman M. Optical Spectra and Electronic Structure of Porphyrins and Related Rings. In The Porphyrins, vol. III, Dolphin D. (Ed.) Academic Press: New York, 1978, 1-165.

[6] (a) Zhao Z, Cammidge AN and Cook MJ. Chem. *Commun.* 2009; 7530-7532. (b) Zhao Z, Cammidge AM, Hughes DL and Cook MJ. *Org. Lett*. 2010; **12**: 5138-5141.

[7] Awasthi K, Nakamur K, Kono H, Kobayashi N and Ohta N. *Chem. Phys. Lett.* 2014; **599**: 163-168.

[8] Claessens CG, González-Rodríguez D and Torres T. *Chem. Rev.* 2002; **102**: 835-853.

[9] del Rey B, Keller U, Torres T, Rojo G, Agulló-López F, Nonell S, Marti C, Brasselet S, Ledoux I and Zyss J. *J. Am. Chem. Soc.* 1998; **120**: 12808-12817.

[10] Mack J, Otaki T, Durfee WS, Kobayashi N and Stillman MJ. *J. Inorg. Biochem.* 2014; **136**: 122-129.

[11] Humphrey JL, and Kuciauskas D. *J. Phys. Chem. C* 2008: **112**; 1700-1704.

[12] (a) Claessens CG, González-Rodríguez D and Torres T. *Chem. Rev.* 2002; **102**: 835-853. (b) Geyer M, Plenzig F, Rauschnabel J, Hanack M, del Rey B, Sastre A and Torres T. *Synthesis* 1996; 1139-1151.

[13] Silva S, Pereira PMR, Silva P, Almeida Paz FA, Faustino MAF, Caveleiro JAS and Tome JPC, *Chem. Comm.* 2012; **48**: 3608-3610.

[14] (a) F. D'Souza, S. Gadde, M. E. Zandler, K. Arkady, M. E. El-Khouly, M. Fujitsuka, O. Ito, *J. Phys. Chem. A* 2002; **106**: 12393-12404. (b) T. Ogi, H. Ohkita, S. Ito, M. Yamamoto, *Thin Solid Films* 2002; **415**: 228-235. (c) A. Felgenträger, T. Maisch, A. Späth, J. A. Schröder, W. Bäumler, *Phys. Chem. Chem. Phys.*, 2014; **16**: 20598-20607.

[15] Piepho SB and Schatz PN. Group Theory in Spectroscopy with Applications to Magnetic Circular Dichroism, Wiley: New York, 1983.

[16] Gaussian 09, Revision A.02, Frisch MJ, Trucks GW, Schlegel HB, Scuseria GE, Robb MA, Cheeseman JR, Scalmani G, Barone V, Mennucci B, Petersson GA, Nakatsuji H, Caricato M, Li X, Hratchian HP, Izmaylov AF, Bloino J, Zheng G, Sonnenberg JL, Hada M, Ehara M, Toyota K, Fukuda R, Hasegawa J, Ishida M, Nakajima T, Honda Y, Kitao O, Nakai H, Vreven T, Montgomery JA, Jr, Peralta JE, Ogliaro F, Bearpark M, Heyd JJ, Brothers E, Kudin KN, Staroverov VN, Kobayashi R, Normand J, Raghavachari K, Rendell A, Burant JC, Iyengar SS, Tomasi J, Cossi M, Rega N, Millam JM, Klene M, Knox JE, Cross JB, Bakken V, Adamo C, Jaramillo J, Gomperts R, Stratmann RE, Yazyev O, Austin AJ, Cammi R, Pomelli C, Ochterski JW, Martin RL, Morokuma K, Zakrzewski VG, Voth GA, Salvador P, Dannenberg JJ, Dapprich S, Daniels AD, Farkas Ö, Foresman JB, Ortiz JV, Cioslowski J and Fox DJ. Gaussian, Inc., Wallingford CT, 2009.

[17] (a) Michl J. *J. Am. Chem. Soc.* 1978; **100**: 6801-6811. (b) Michl J. *J. Am. Chem. Soc.* 1978, **100**: 6812-6818. (c) Michl J. *Pure Appl. Chem.* 1980, **52**: 1549-1563. (d) Michl J. *Tetrahedron* 1984, **40**: 3845-3934.

[18] Viswanath CLK, Shirtcliff DL and Berlin SKKD. *Dyes Pigments* 2015; **112**: 283-289.

[19] Ito T, Hayashi Y, Shimizu S, Shin J-Y, Kobayashi N and Shinokubo H. *Angew. Chem. Int. Ed.* 2012; **51**: 8542-8545.

[20] Mack J, Stillman MJ and Kobayashi N, *Coord. Chem. Rev*. 2007, **251**: 429-453.

[21] Kobayashi N, Muranaka A and Mack J. *Circular Dichroism and Magnetic Circular Dichroism Spectroscopy for Organic Chemists*, Royal Society of Chemistry: London, UK, 2011.

[22] Mack J, Asano Y, Kobayashi N and Stillman MJ. *J. Am. Chem. Soc.* 2005; **127**: 17697-17711.

[23] Patterson MS, Madsen SJ and Wilson R. *J. Photochem. Photobiol. B* 1990: **5**; 69

[24] (a) R. W. Redmond, J. N. Gamlin, *J. Photochem. Photobiol.* 1999, **70**, 391-475. (b) U. Michelsen, H. Kliesch, G. Schnurpfeil, A. K. Sobbi, D. Wöhrle, *Photochem. Photobiol.* 1996; **64**: 694-701.

[25] S. Fery-Forgues, D. Lavabre, *J. Chem. Ed.* 1999; **76**: 1260-1264.

[26] Seybold PG and Gouterman M. *J. Mol. Spectrosc.* 1969; **31**: 1-13.

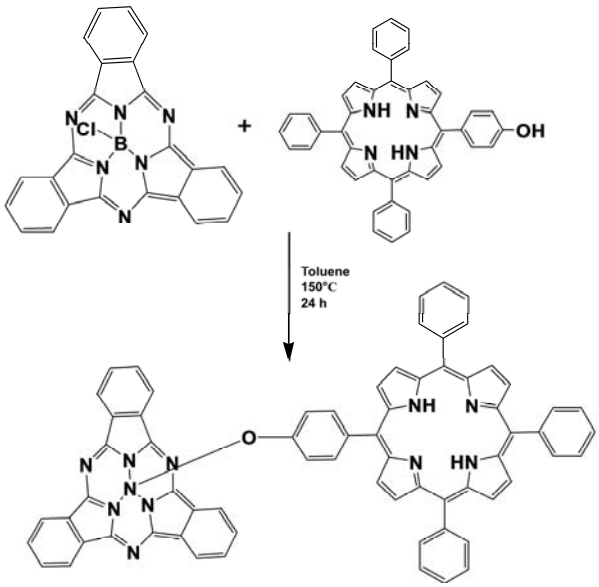

Scheme 1. Synthetic scheme for the formation of **H_2TPP-O-subPc**.

Figures

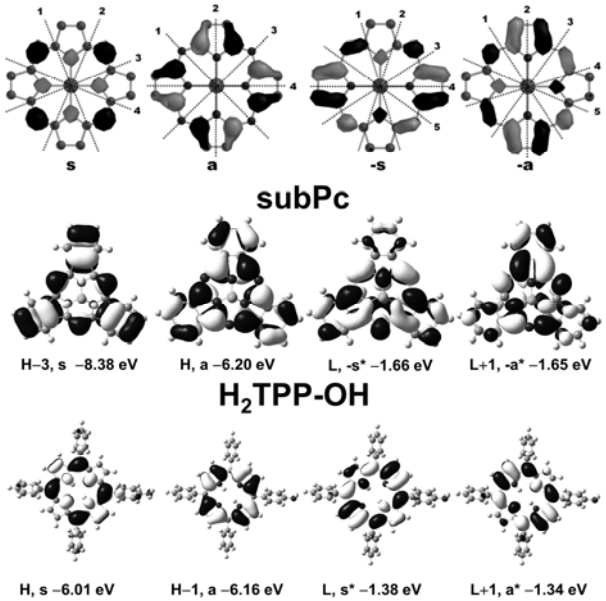

Figure 1 Nodal patterns and energies of the frontier π-MOs of **subPc** (CENTER) and **H_2TPP-OH** (BOTTOM) at an isosurface value of 0.02 a.u. H and L denote the HOMO and LUMO, respectively. Nodal patterns of the four frontier π-MOs of tetrapyrrolic porphyrins (TOP). Michl [17] introduced the **a**, **s**, **-a** and **-s** nomenclature to describe the four frontier π-MOs with $M_L = \pm 4$ and ± 5 nodal patterns based on whether there is a nodal plane (**a** and **-a**) or an antinode (**s** and **-s**) on the *y*-axis. This makes it easier to compare MOs of porphyrin complexes with differing symmetries (Table 1).

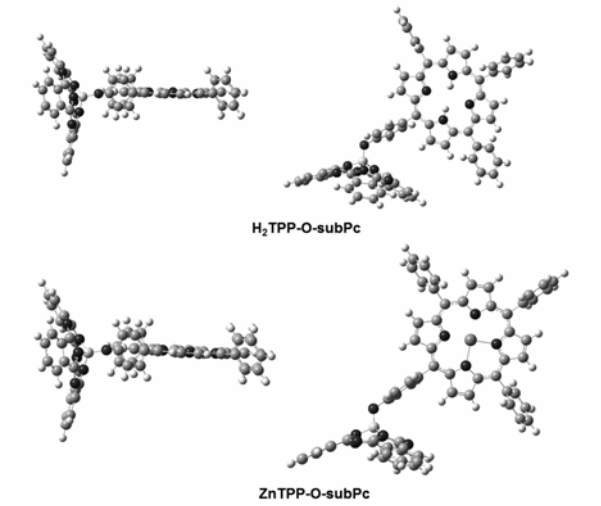

Fig. 2. B3LYP optimized geometries of **H_2TPP-O-subPc** and **ZnTPP-O-subPc**.

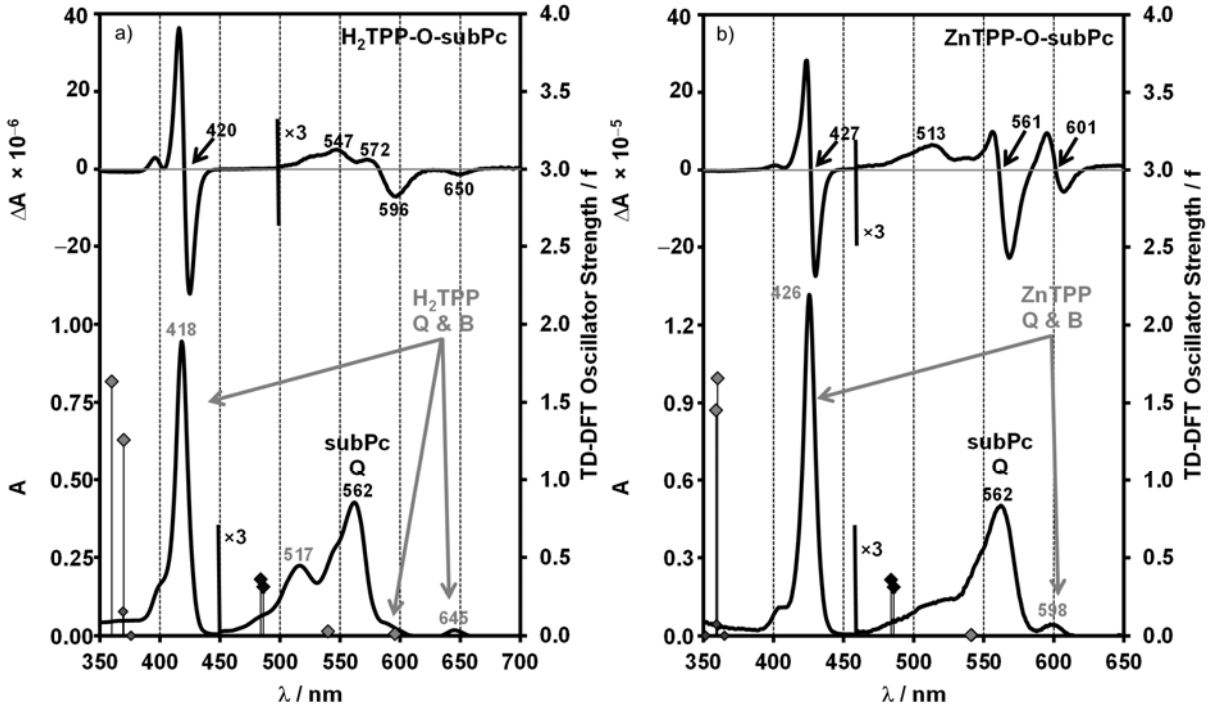

Fig. 3. UV-visible absorption and MCD spectra of a) **H_2TPP-O-subPc** and b) **ZnTPP-O-subPc**. The calculated TD-DFT spectra calculated using the CAM-B3LYP functionals with 6-31G(d) basis sets and are plotted against a secondary right-hand axis. Large gray and black diamonds are used to highlight the Q and B bands of the TPP and subPc moieties. Smaller diamonds are used for other transitions.

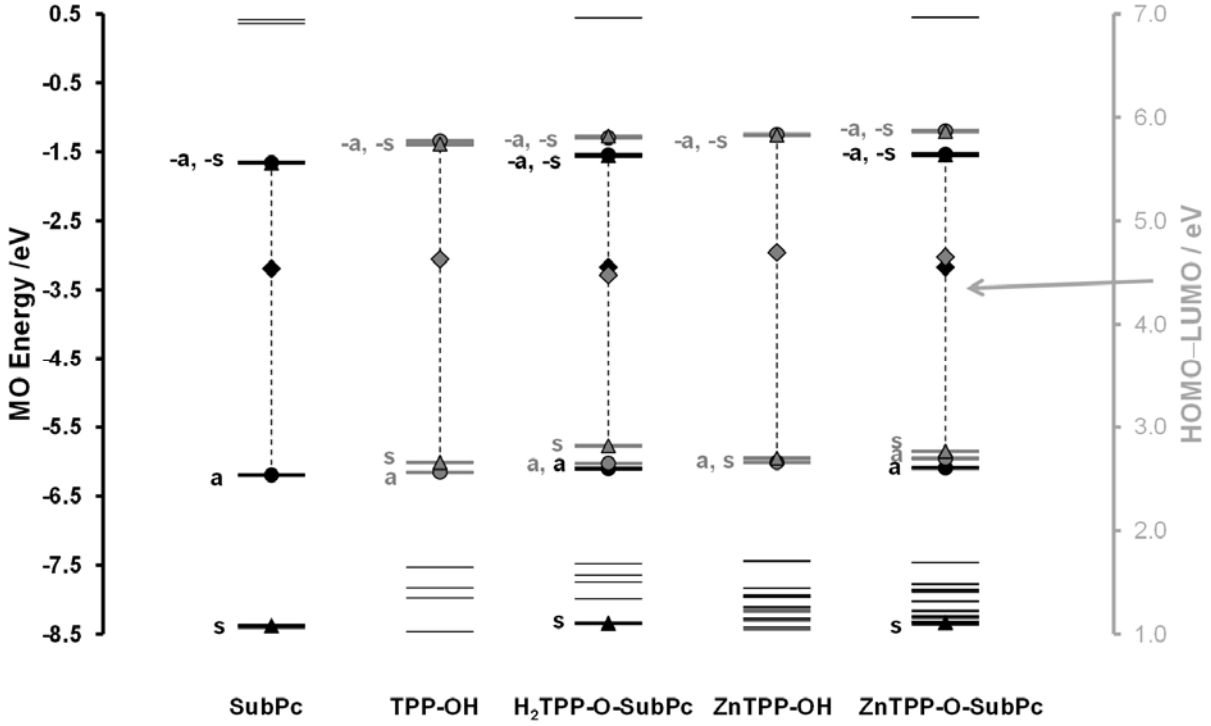

Fig. 4. MO energies of **subPc**, **H_2TPP-OH**, **H_2TPP-O-subPc**, **ZnTPP-OH** and **ZnTPP-O-subPc** in the TD-DFT calculations carried out using the CAM-B3LYP functional with 6-31G(d) basis sets. The **a**, **s**, **-a** and **-s** MOs of the TPP and subPc chromophores are highlighted with gray and black lines, respectively. Triangles and circles are used to denote the **s**/**-s** and **a**/**-a** MOs. The HOMO–LUMO gaps for the TPP and subPc moieties are denoted with gray and black diamonds, respectively, and are plotted against a secondary axis.

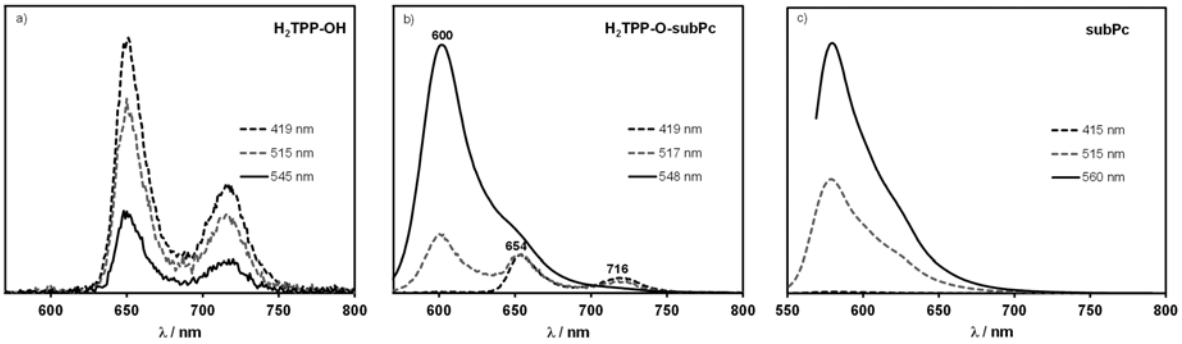

Fig. 5. Excitation wavelength dependence of the fluorescence emission spectra of a) **H_2TPP-OH**, b) **ZnTPP-O-subPc** and c) **subPc**.

TABLES

Table 1. The photophysical properties of **subPc**, **H_2TPP-OH**, **H_2TPP-O-subPc**, **ZnTPP-OH** and **ZnTPP-O-subPc** in DMF.

	Abs (nm)	**(Φ_Δ)**	**(Φ_F)**
subPc	304 (B), 562 (Q)	λ_{ex} = 566 nm, 0.76	λ_{ex} = 415 nm, 0.21
H_2TPP-OH	417 (B), 513, 548, 590, 646 (Q)	λ_{ex} = 417 nm, 0.57	λ_{ex} = 417 nm, 0.19
H_2TPP-O-SubPc	418 (B), 515, 562, 645 (Q)	λ_{ex} = 418 nm, 0.55	λ_{ex} = 415 nm, 0.055
		λ_{ex} = 562 nm, 0.69	λ_{ex} = 515 nm, 0.13
			λ_{ex} = 569 nm, 0.12
ZnTPP-OH	425 (B), 556, 599 (Q)	λ_{ex} = 425 nm, 0.75	λ_{ex} = 425 nm, 0.13
ZnTPP-O-SubPc	426 (B), 562, 598 (Q)	λ_{ex} = 426 nm, 0.50	λ_{ex} = 425 nm, 0.046
		λ_{ex} = 532 nm, 0.72	λ_{ex} = 515 nm, 0.12
			λ_{ex} = 569 nm, 0.10

Table 2. TD-DFT spectra of the B3LYP optimized geometries in the 350–700 nm region for **subPc**, **H_2TPP-OH**, **ZnTPP-OH**, **H_2TPP-O-subPc** and **ZnTPP-O-subPc** calculated with the CAM-B3LYP functional and 6-31G(d) basis sets.

Band[a]	#[b]	Calc[c]			Exp[d]		Wavefunction=[e]
subPc							
Q	**2**	20.5	487	0.34	17.8	562	**94% a → -s**; …
	3	20.6	486	0.34			**94% a → -a**; …
H_2TPP-OH							
Q	**2**	16.7	599	0.01	15.4	646	**59% s → -s**; **38% a → -a**; …
	3	18.4	543	0.03	18.2	548	**58% s → -a**; **39% a → -s**; …
B	**4**	27.0	370	1.31	23.8	417	**57% a → -a**; **31% s → -s**; …
	5	27.7	361	1.67			**58% a → -s**; **38% s → -a**; …
ZnTPP-OH							
Q	**2**	18.3	545	0.01	16.7	599	**52% s → -a**; **43% a → -s**; …
	3	18.3	545	0.01			**52% s → -s**; **44% a → -a**; …
B	**4**	27.5	363	1.50	23.5	425	**53% a → -a**; **42% s → -s**; …
	5	27.6	363	1.45			**54% a → -s**; **41% s → -a**; …
H_2TPP-O-subPc							
Q^{TPP}	**2**	16.8	596	0.01	15.5	645	**56% s → -s**; **38% a → -a**; …
	3	18.5	540	0.03	---	---	**55% s → -a**; **39% a → -s**; …
Q^{sub}	**4**	20.6	486	0.31	17.8	562	**94% a → -s**; …
	5	20.7	484	0.36			**94% a → -a**; …
B^{TPP}	**7**	27.0	370	1.26	23.9	418	**49% a → -a**; **30% s → -s**; 11% $s^{TPP} \rightarrow -a^{subPc}$; …
	9	27.8	360	1.63			**58% a → -s**; **41% s → -a**; …
ZnTPP-O-subPc							
Q^{TPP}	**2**	18.5	541	0.01	16.7	598	**52% s → -a**; **46% a → -s**; …
	3	18.5	541	0.01			**52% s → -s**; **47% a → -a**; …
Q^{sub}	**4**	20.6	486	0.31	17.8	562	**94% a → -s**; …
	5	20.7	484	0.36			**94% a → -a**; …
B^{TPP}	**7**	27.8	360	1.66	23.5	426	**50% a → -s**; **44% s → -a**; …
	9	27.9	359	1.45			**53% a → -a**; **46% s → -s**; …

[a] − Band assignment described in the text. [b] − The number of the state assigned in terms of ascending energy within the TD-DFT calculation. [c] − Calculated band energies ($10^3.cm^{-1}$), wavelengths (nm) and oscillator strengths in parentheses (f). [d] − Observed energies ($10^3.cm^{-1}$) and wavelengths (nm). [e] − The wave functions based on the eigenvectors predicted by TD-DFT. One-electron transitions associated with the four frontier π-MOs of Gouterman's 4-orbital model [5] are highlighted in bold. H and L refer to the HOMO and LUMO, respectively. Michl's **a**, **s**, **-a** and **-s** nomenclature for the four frontier π-MOs [17] is used to facilitate comparison of the transition of porphyrinoids with differing symmetries.